Electronic Supplementary Material (ESI) for Dalton Transactions.

Supplementary Information

Featuring long-lifetime deep-red emitting iridium^{III} complexes with high colour purity: insights on the excited state dynamics from spectroscopic and theoretical perspectives

Renan C. Silva[a,b], Felipe S. M. Canisares[c], Leonardo F. Saraiva[a,b], Ana M. Pires[a,b,c], Sergio A. M. Lima[a,b,c]

[a] São Paulo State University (Unesp), Institute of Biosciences, Humanities and Exact Sciences, São José do Rio Preto-SP, Brazil.

[b] São Paulo State University (Unesp), School of Technology and Sciences, Presidente Prudente-SP, Brazil.

[c] São Paulo State University (Unesp), Institute of Chemistry, Araraquara-SP, Brazil.

Table of Contents

Supplementary Notes S1: State of the art of deep-red emitting iridium^{III} complexes

Table S1. State-of-the-art of iridium^{III} complexes applied to optical oxygen sensors probes.

Complex	$\lambda_{em/nm}$	SWHM[d]/nm	Φ/%	$\tau_{obs/\mu s}$	Ref.
Ir-pb	645	603–714	34.0	1.13	This work[e]
Ir-qb	625	570–695	10.6	1.11	
Ir-bb	631	589–699	26.6	1.72	
[Ir(N^C1)$_2$(N^12)](PF$_6$)[a]	717, 784, 885sh	-	13.6	3.32	1
[Ir(N^C1)$_2$(N^N2)](PF$_6$)[a]	715, 779, 875sh	-	12.9	2.34	
[Ir(N^C1)$_2$(N^N3)](PF$_6$)[a]	713, 778, 880sh	-	10.3	1.76	
[Ir(N^C1)$_2$(N^N4)](PF$_6$)[a]	713, 779, 870sh	-	12.7	2.22	
[Ir(N^C2)$_2$(N^N1)](PF$_6$)[a]	720, 790, 890sh	-	12.2	3.37	
[Ir(N^C3)$_2$(N^N1)](PF$_6$)[a]	722, 785, 985sh	-	11.1	3.18	
[Ir(N^C4)$_2$(N^N1)](PF$_6$)[a]	720, 783, 890sh	-	20.5	5.59	
[Ir(btq)$_2$(acac)][b]	672	650–700	1.40	0.13	2
[Ir(btq)$_2$(phen-NH$_2$)][b]	655	625–725	1.90	0.35	
[Ir(btq)$_2$(phen-DEA)][b]	657	630–725	2.10	0.36	
[Ir(ttph)$_2$(acac)][b]	693	675–775	2.20	0.38	
[Ir(ttph)$_2$(phen-NH$_2$)][b]	686	660–775	2.60	0.23	
[Ir(ttph)$_2$(phen-DMA)][b]	688	660–780	1.70	0.44	
[Ir(btph)$_2$(acac)][b]	718	700–750	3.60	0.24	
[Ir(btph)$_2$(phen-NH$_2$)][b]	710	690–790	2.40	0.39	
[Ir(btph)$_2$(phen-DMA)][b]	711	690–790	2.50	0.40	
[Ir(L1)$_2$(pic)][c]	647	615-690	4.10	0.30	3
[Ir(L2)$_2$(pic)][c]	640	610-687	6.80	0.29	
[Ir(L3)$_2$(pic)][c]	665	630-715	3.60	0.27	
[Ir(L4)$_2$(pic)][c]	650	620-705	3.30	0.29	
[Ir(L5)$_2$(pic)][c]	648	620-690	3.10	0.31	
[Ir(L6)$_2$(pic)][c]	680	637-720	3.40	0.29	
[Ir(L7)$_2$(pic)][c]	653	630-710	3.30	0.29	
[Ir(L2)$_2$(pyz)][c]	633	605-680	2.70	0.35	
[Ir(L5)$_2$(pyz)][c]	641	615-685	3.00	0.33	
[Ir(L7)$_2$(pyz)][c]	651	625-700	2.80	0.35	

[a]deoxygenated methanol solution. [b]aerated toluene solution. [c]aerated chloroform solution. [d]Spectral Window at Half Maximum. [e]quantum yield and lifetime measured in deoxygenated DMSO solution.

Supplementary Notes S2: FTIR Analysis

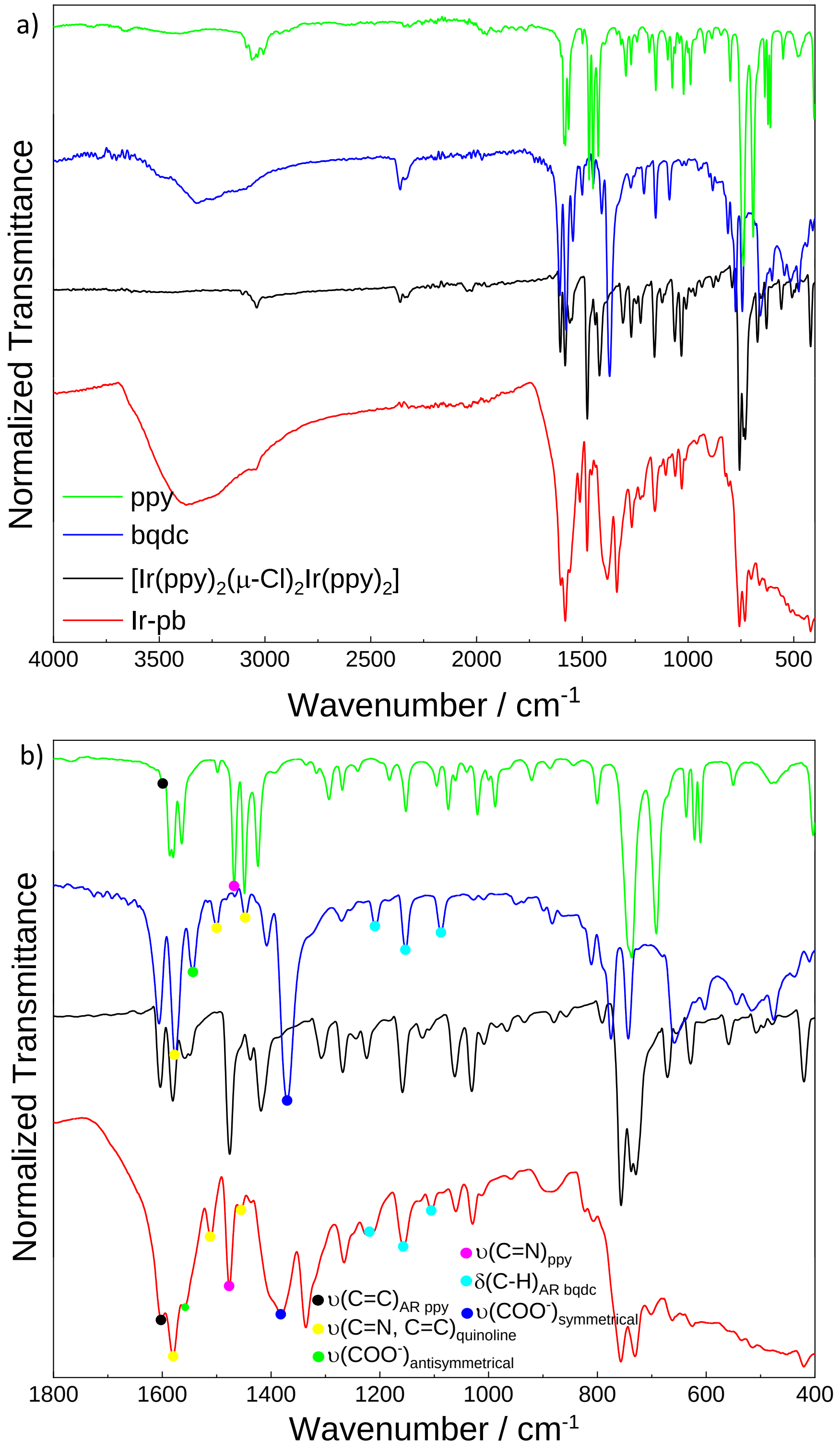

Fig. S1. FTIR spectra in the 4000 – 400 cm^{-1} range (a) and magnification of the region between 1800 – 400 cm^{-1} (b) of the complex **Ir-pb** and its respective precursors.

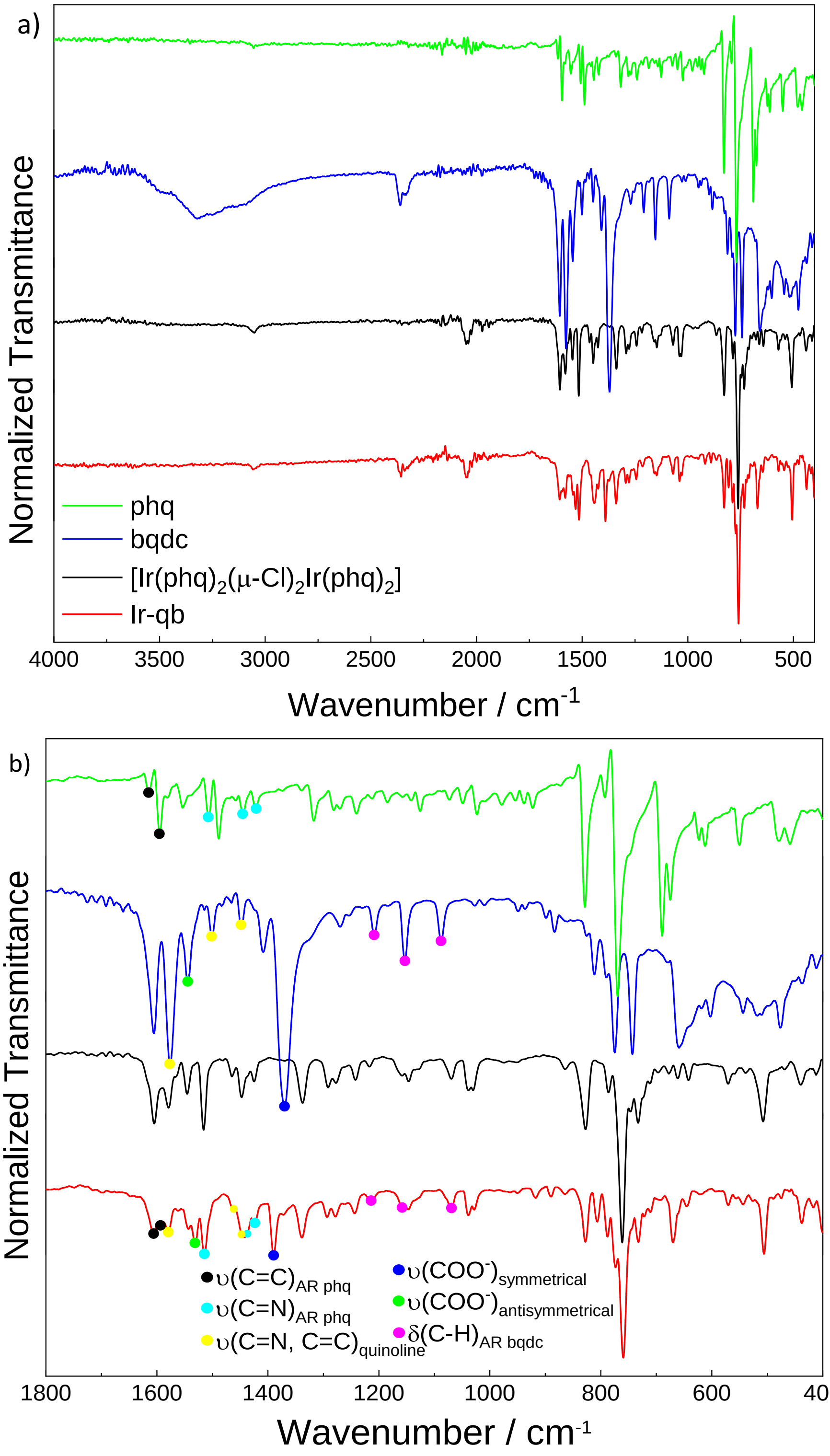

Fig S2. FTIR spectra in the 4000 – 400 cm^{-1} range (a) and magnification of the region between 1800 – 400 cm^{-1} (b) of the complex **Ir-qb** and its respective precursors.

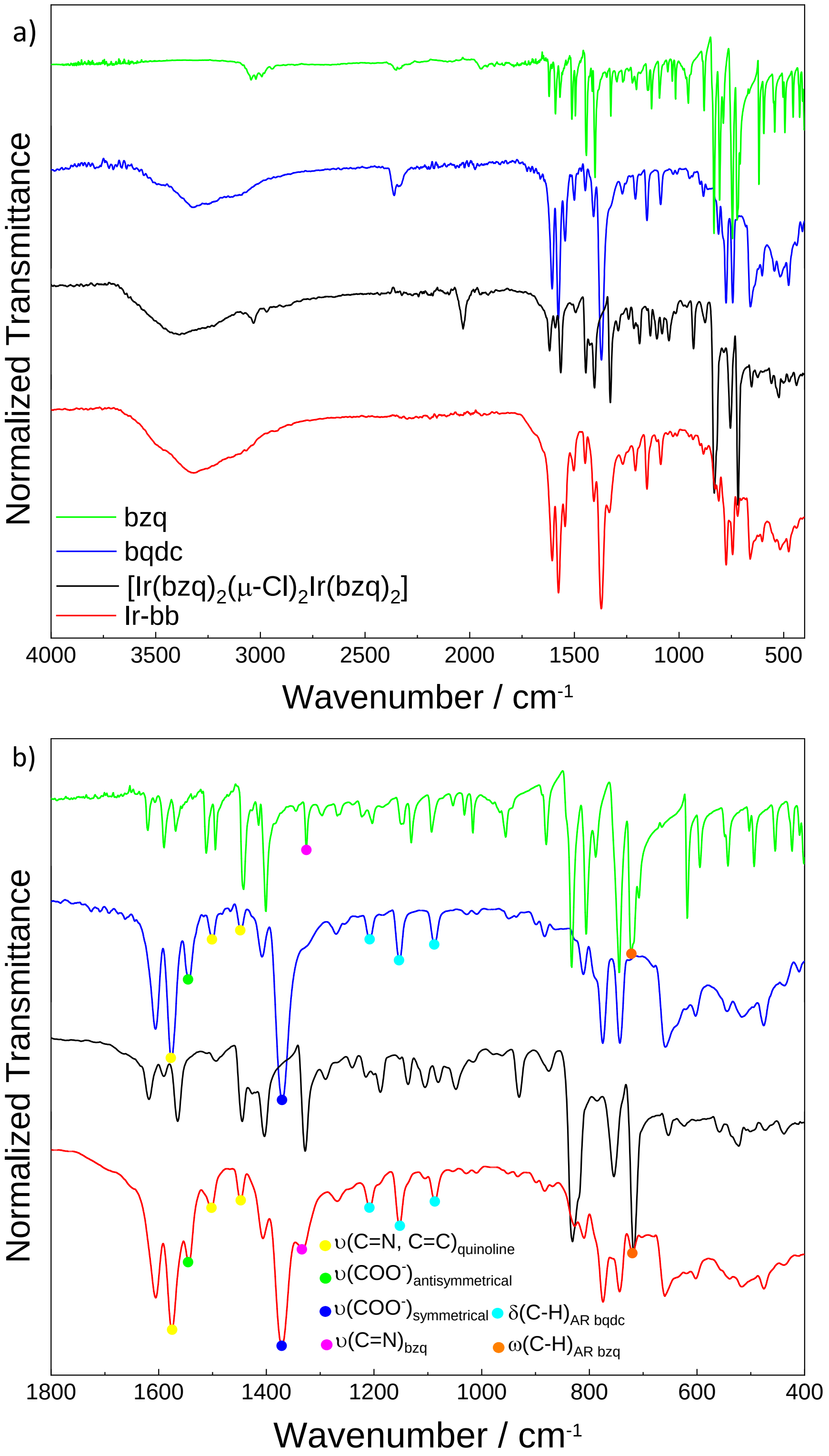

Fig. S3. FTIR spectra in the 4000 – 400 cm^{-1} range (a) and magnification of the region between 1800 – 400 cm^{-1} (b) of the complex **Ir-bb** and its respective precursors.

Table S2. Main vibrational modes (cm^{-1}) attributed to Ir^{III} complexes and their precursors.

Assignments	Ir-pb	ppy	bqdc
υ(C=C)$_{\text{AR ppy}}$	1602	1599	-
υ(C=N, C=C)$_{\text{quinoline}}$	1580	-	1576
	1510		1499
	1455		1447
υ(C=N)$_{\text{AR ppy}}$	1477	1468	-
υ(COO$^-$)$_{\text{antisymmetrical}}$	1558	-	1543
υ(COO$^-$)$_{\text{symmetrical}}$	1382	-	1370
δ(C-H)$_{\text{AR bqdc}}$	1219	-	1208
	1157		1153
	1105		1087

Assignments	Ir-qb	phq	bqdc
u(C=C)$_{\text{AR phq}}$	1606	1615	-
	1593	1595	
υ(C=N, C=C)$_{\text{quinoline}}$	1579	-	1576
	1463		1499
	1447		1447
υ(C=N)$_{\text{AR phq}}$	1514	1507	-
	1437	1445	
	1423	1422	
υ(COO$^-$)$_{\text{antisymmetrical}}$	1579	-	1543
υ(COO$^-$)$_{\text{symmetrical}}$	1389	-	1370
δ(C-H)$_{\text{AR bqdc}}$	1214	-	1208
	1158		1153
	1070		1087

Assignments	Ir-bb	bzq	bqdc
υ(C=N, C=C)$_{\text{quinoline}}$	1575	-	1576
	1502		1499
	1448		1447
υ(C=N)$_{\text{AR bzq}}$	1333	1326	-
υ(COO$^-$)$_{\text{antisymmetrical}}$	1544	-	1543
υ(COO$^-$)$_{\text{symmetrical}}$	1373	-	1370
δ(C-H)$_{\text{AR bqdc}}$	1208	-	1208
	1152		1153
	1087		1087
ω(C-H)$_{\text{AR bzq}}$	720	717	-

υ = Stretching; δ = deformation in plane, ω = deformation out of plane.

Supplementary Notes S3: ^{1}H-NMR Analysis

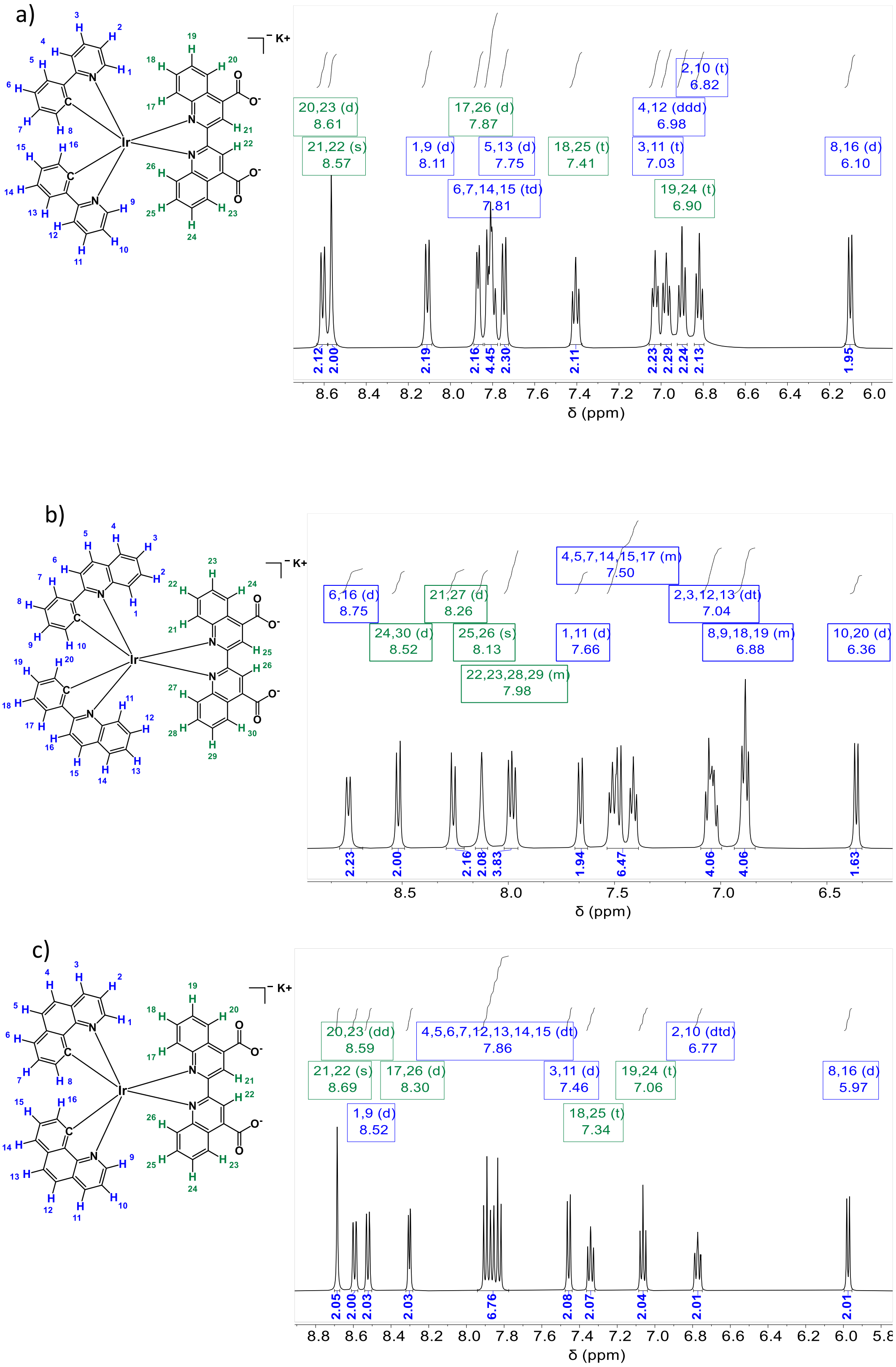

Fig. S4. ^{1}H-NMR spectra of **Ir-pb** (a), **Ir-qb** (b), and **Ir-bb** (c) in DMSO-d_6. (500 MHz, T = 298 K).

Supplementary Notes S4: MALDI-TOF Analysis

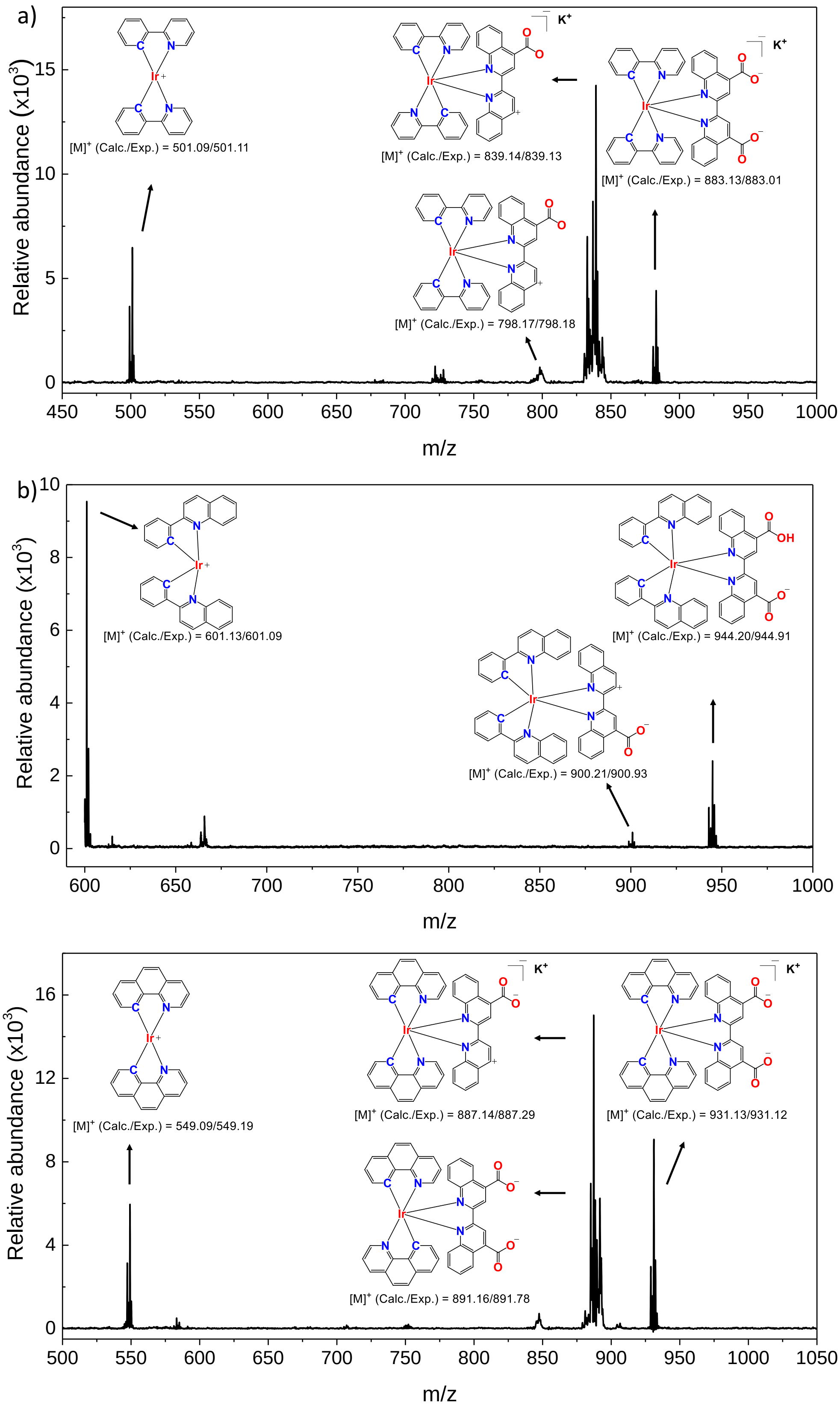

Fig. S5. MALDI-TOF mass spectra of the heteroleptic complexes **Ir-pb** (a), **Ir-qb** (b) and **Ir-bb** (c).

Supplementary Notes S5: UV-Vis Spectroscopy Analysis

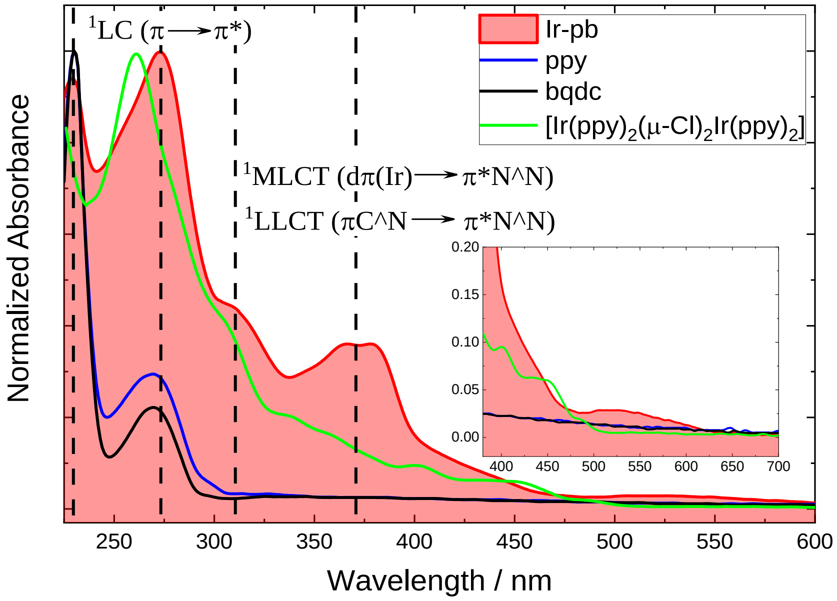

Fig. S6. UV-Vis absorption spectra of the complex **Ir-pb** (red area) and precursor ligands ppy (blue line), bqdc (black line), and dimer (green line) in DCM 1.0×10^{-5} mol L^{-1} at 298 K.

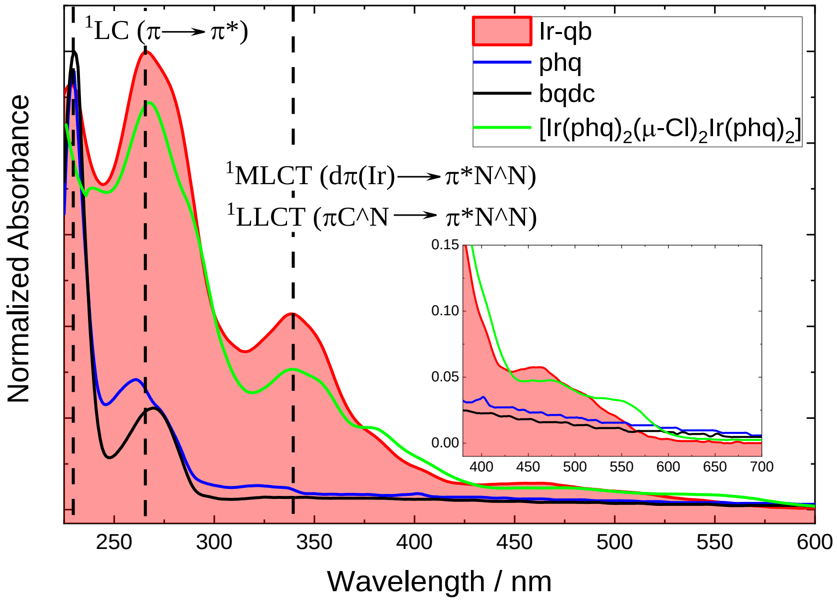

Fig. S7. UV-Vis absorption spectra of the complex **Ir-qb** (red area) and precursor ligands phq (blue line), bqdc (black line), and dimer (green line) in DCM 1.0×10^{-5} mol L^{-1} at 298 K.

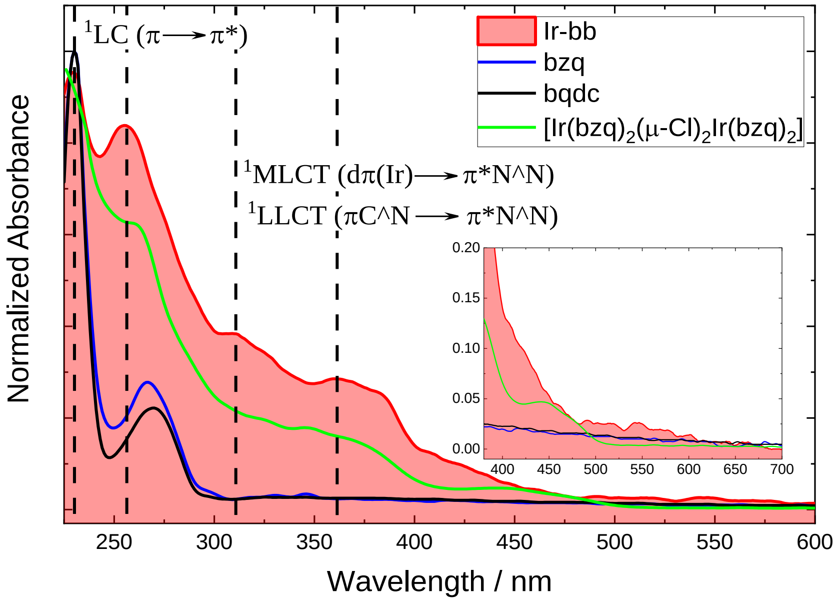

Fig. S8. UV-Vis absorption spectra of the complex **Ir-bb** (red area) and precursor ligands bzq (blue line), bqdc (black line), and dimer (green line) in DCM 1.0×10^{-5} mol L^{-1} at 298 K.

Supplementary Notes S6: Cyclic Voltammetry and Energy Level Determination

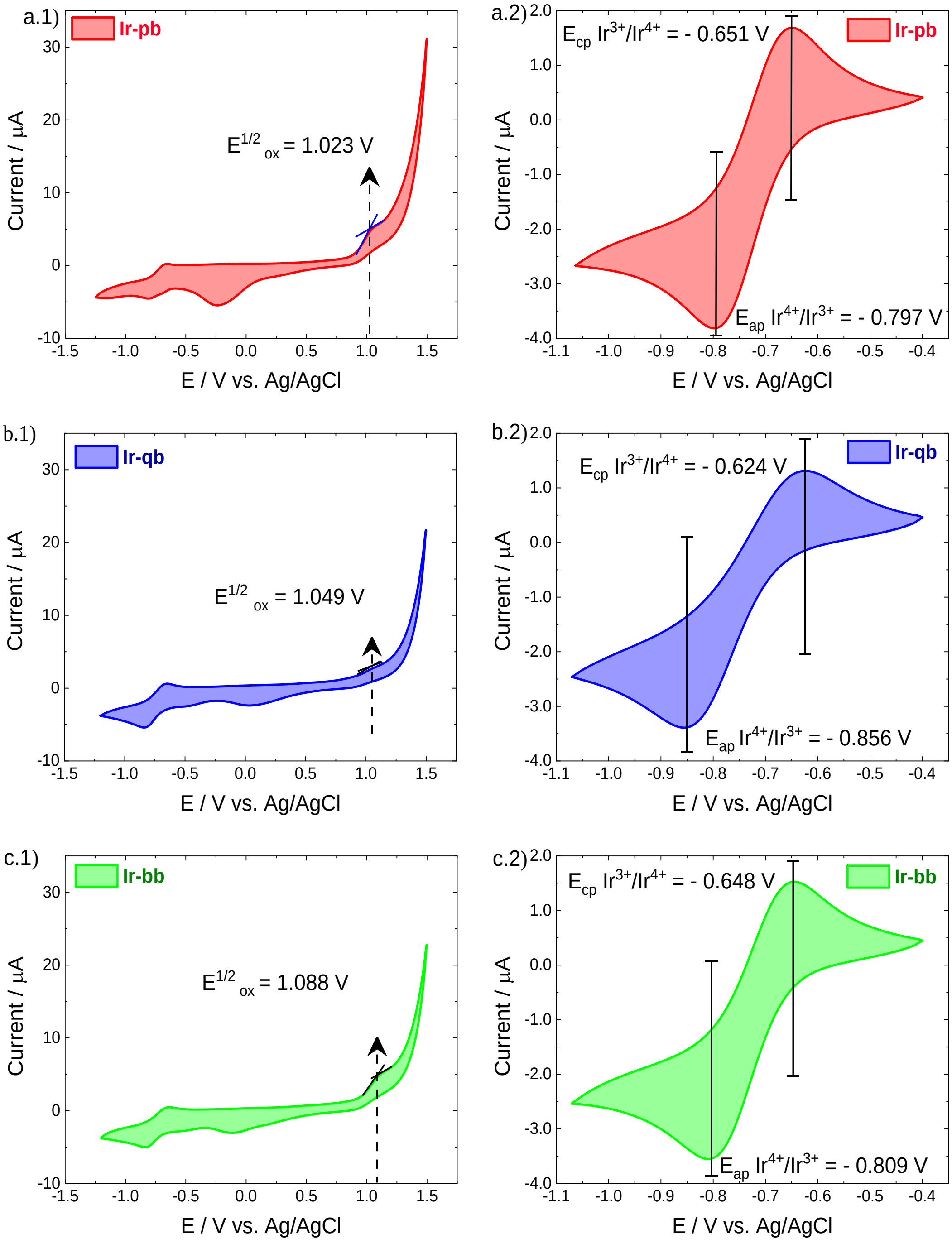

Fig. S9. Cyclic voltammograms of the investigated Ir^{III} complexes in DMSO (1.0×10^{-4} mol L^{-1}) with n-Bu_4NPF_6 (0.10 mol L^{-1}) as the supporting electrolyte and using ferrocene as the standard. The full scan occurred between – 1.200 to + 1.500 V for **Ir-pb** (a.1), **Ir-qb** (b.1) and **Ir-bb** (c.1). Extended area between – 1.000 to – 0.400 V showing the possible reversible process Ir^{4+}/Ir^{3+} for **Ir-pb** (a.2), **Ir-qb** (b.2) and **Ir-bb** (c.2).

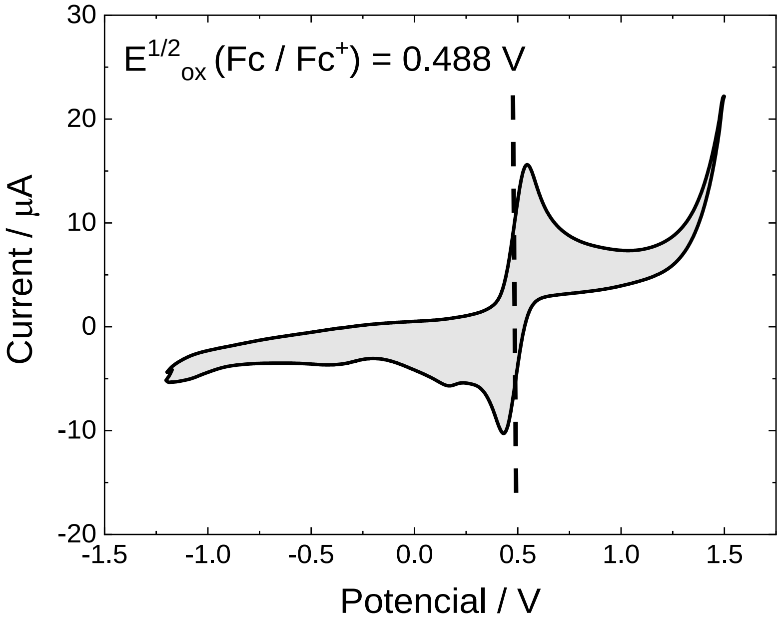

Fig. S10. Cyclic voltammogram of ferrocene.

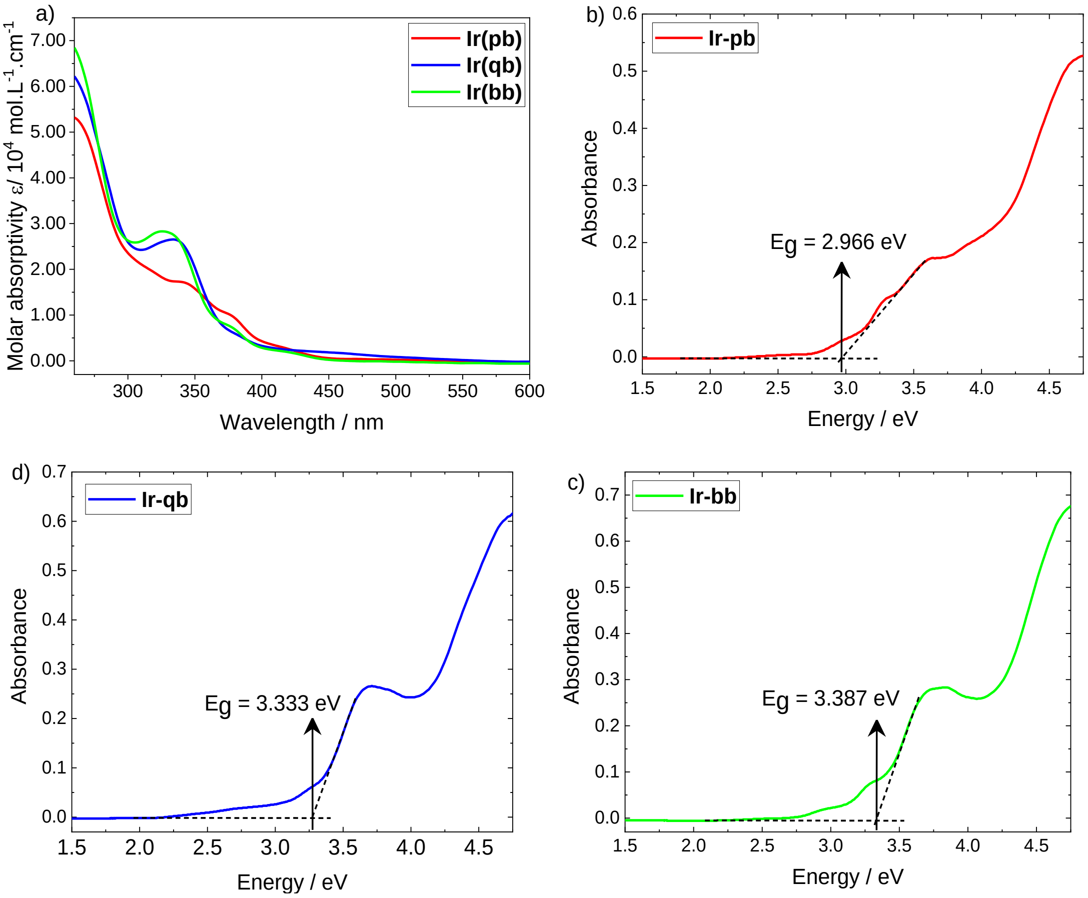

Fig. S11. Absorption spectra in the UV-Vis region of complexes in DMSO solution at 1.0×10^{-5} mol L^{-1} (a). Determination of the optical energy gap (Eg) through the onset wavelengths of the absorption spectra in DMSO at 1.0×10^{-5} mol L^{-1}, **Ir-pb** (b), **Ir-qb** (c), and **Ir-bb** (d).

Supplementary Notes S7 Theoretical Density Functional Calculations of Electronic Structure

Table S3. Electron Density Populations of Molecular Orbitals (%) of the metal and each ligand to the composition of selected molecular orbitals.

Orbital	Ir-pb			Ir-qb			Ir-bb		
	Ir^{III}	*ppy*	*bqdc*	Ir^{III}	*phq*	*bqdc*	Ir^{III}	*bzq*	*bqdc*
LUMO+1	6.38	78.9	14.7	17.8	71.3	13.8	2.21	70.8	26.9
LUMO	3.45	18.5	**78.9**	3.68	29.2	**67.1**	4.44	26.3	**69.2**
HOMO	**38.6**	**39.2**	22.0	**38.6**	**41.6**	19.7	**36.9**	**45.1**	17.9
HOMO-1	28.4	46.9	24.6	24.0	41.2	34.8	31.7	43.2	25.1
HOMO-2	40.4	40.7	18.7	24.3	55.0	20.5	19.7	13.4	60.9

Table S4. The contribution of HOMOs-LUMOs for four calculated states.

State	Ir-pb	Ir-qb	Ir-bb
	Transition (Contribution %)		
1	HOMO-18→LUMO (1.21)	HOMO-2→LUMO (1.66)	HOMO-10→LUMO (3.45)
	HOMO-17→LUMO (1.07)	HOMO-3→LUMO (1.87)	HOMO-9→LUMO (1.36)
	HOMO-16→LUMO (1.47)	HOMO-1→LUMO (3.85)	HOMO-3→LUMO (7.03)
	HOMO-3→LUMO (1.75)	HOMO→LUMO (80.41)	HOMO-1→LUMO (2.82)
	HOMO-1→LUMO (2.25)		HOMO→LUMO (75.6)
	HOMO→LUMO (83.44)		
2	HOMO-10→LUMO (2.17)	HOMO-16→LUMO (2.26)	HOMO-12→LUMO (1.55)
	HOMO-2→LUMO (12.13)	HOMO-13→LUMO (1.61)	HOMO-10→LUMO (2.04)
	HOMO-1→LUMO (70.39)	HOMO-4→LUMO (1.48)	HOMO-4→LUMO (1.20)
	HOMO→LUMO (3.22)	HOMO-2→LUMO (6.75)	HOMO-2→LUMO (17.28)
		HOMO-1→LUMO (69.81)	HOMO-1→LUMO (62.15)
		HOMO→LUMO (5.06)	HOMO→LUMO (4.18)
3	HOMO-12→LUMO (5.03)	HOMO-6→LUMO (1.18)	HOMO-13→LUMO (3.08)
	HOMO-9→LUMO (1.18)	HOMO-4→LUMO (1.31)	HOMO-11→LUMO (2.48)
	HOMO-7→LUMO (1.22)	HOMO-3→LUMO (1.38)	HOMO-10→LUMO (6.26)
	HOMO-4→LUMO (6.60)	HOMO-1→LUMO (1.48)	HOMO-7→LUMO (2.73)
	HOMO-3→LUMO (1.54)	HOMO-1→LUMO+1 (13.70)	HOMO-4→LUMO (9.86)
	HOMO-2→LUMO (63.18)	HOMO→LUMO+1 (68.33)	HOMO-3→LUMO (2.21)
	HOMO-1→LUMO (10.87)		HOMO-2→LUMO (52.40)
	HOMO-12→LUMO (5.03)		HOMO-1→LUMO (10.57)
4	HOMO-3→LUMO+1 (2.44)	HOMO-16→LUMO (2.42)	HOMO-6→LUMO+1 (4.01)
	HOMO-1→LUMO+1 (11.64)	HOMO-13→LUMO (3.71)	HOMO-4→LUMO+4 (1.25)
	HOMO→LUMO+1 (71.99)	HOMO-11→LUMO (1.44)	HOMO-1→LUMO+1 (17.35)
	HOMO→LUMO+3 (2.03)	HOMO-8→LUMO (2.03)	HOMO-1→LUMO+4 (2.64)
		HOMO-5→LUMO (7.66)	HOMO-1→LUMO+5 (1.41)
		HOMO-4→LUMO (1.65)	HOMO→LUMO+1 (56.7)
		HOMO-3→LUMO (10.38)	HOMO→LUMO+4 (2.59)
		HOMO-2→LUMO (44.07)	HOMO→LUMO+5 (1.06)
		HOMO-1→LUMO (5.30)	
		HOMO-1→LUMO+2 (2.06)	
		HOMO→LUMO+2 (6.19)	

Table S5. Calculated spin-orbit coupling matrix elements between triplets (T) and singlets (S) using ωB97x-D4 functional for the complex **Ir-pb**.

Root		$\langle \mathrm{T}\vert \mathrm{H_{SO}}\vert \mathrm{S}\rangle$ (Re, Im) / cm^{-1}		
T	**S**	**Z**	**X**	**Y**
1	**0**	(0.000, 156.76)	(0.000, -59.52)	(-0.000, 54.99)
1	**1**	(0.000, 300.42)	(0.000, 714.84)	(-0.000, 124.07)
1	**2**	(0.000, 29.24)	(0.000, 125.43)	(-0.000, 10.33)
1	**3**	(0.000, -496.53)	(0.000, 270.41)	(-0.000, -341.00)
1	**4**	(0.000, -31.76)	(0.000, -90.37)	(-0.000, -25.15)
2	**0**	(0.000, -16.90)	(0.000, 67.30)	(-0.000, 20.94)
2	**1**	(0.000, 50.58)	(0.000, 134.30)	(-0.000, -554.55)
2	**2**	(0.000, 50.48)	(0.000, -960.40)	(-0.000, 92.13)
2	**3**	(0.000, -62.66)	(0.000, -119.28)	(-0.000, 783.95)
2	**4**	(0.000, -7.17)	(0.000, 265.14)	(-0.000, 13.83)
3	**0**	(0.000, 118.29)	(0.000, -18.13)	(-0.000, -569.27)
3	**1**	(0.000, -1.27)	(0.000, -60.96)	(-0.000, 587.50)
3	**2**	(0.000, -898.33)	(0.000, -576.82)	(-0.000, -348.25)
3	**3**	(0.000, -39.22)	(0.000, -142.28)	(-0.000, 832.51)
3	**4**	(0.000, 318.04)	(0.000, 203.94)	(-0.000, 66.90)
4	**0**	(0.000, -291.87)	(0.000, 145.56)	(-0.000, -369.27)
4	**1**	(0.000, 13.70)	(0.000, 80.66)	(-0.000, -51.43)
4	**2**	(0.000, -51.32)	(0.000, -94.05)	(-0.000, -11.48)
4	**3**	(0.000, -59.27)	(0.000, -21.42)	(-0.000, 46.98)
4	**4**	(0.000, 23.07)	(0.000, 31.26)	(-0.000, 11.03)

Table S6. Calculated spin-orbit coupling matrix elements between triplets (T) and singlets (S) using ωB97x-D4 functional for the complex **Ir-qb**.

Root		$\langle \mathrm{T} \vert \mathbf{H}_{\mathrm{SO}} \vert \mathrm{S} \rangle$ **(Re, Im) / cm^{-1}**		
T	**S**	**Z**	**X**	**Y**
1	**0**	(0.000, -144.23)	(0.000, 5.942)	(-0.000, 68.78)
1	**1**	(0.000, 300.52)	(0.000, 714.84)	(-0.000, 407.26)
1	**2**	(0.000, 85.56)	(0.000, 133.81)	(-0.000, -30.52)
1	**3**	(0.000, 71.42)	(0.000, -24.23)	(-0.000, 43.84)
1	**4**	(0.000, 299.01)	(0.000, 322.36)	(-0.000, -51.87)
2	**0**	(0.000, 164.28)	(0.000, -300.04)	(-0.000, 351.88)
2	**1**	(0.000, 83.99)	(0.000, -69.66)	(-0.000, 194.92)
2	**2**	(0.000, 400.11)	(0.000, -461.30)	(-0.000, 117.68)
2	**3**	(0.000, 170.18)	(0.000, -90.22)	(-0.000, 97.71)
2	**4**	(0.000, -10.83)	(0.000, -102.06)	(-0.000, -684.31)
3	**0**	(0.000, 42.24)	(0.000, 96.80)	(-0.000, 343.75)
3	**1**	(0.000, 51.25)	(0.000, 13.14)	(-0.000, -72.41)
3	**2**	(0.000, -53.97)	(0.000, -69.00)	(-0.000, -40.89)
3	**3**	(0.000, -58.29)	(0.000, 102.08)	(-0.000, 104.41)
3	**4**	(0.000, -69.35)	(0.000, -20.42)	(-0.000, -3.75)
4	**0**	(0.000, 293.37)	(0.000, 189.07)	(-0.000, -26.64)
4	**1**	(0.000, 4.32)	(0.000, 208.32)	(-0.000, 49.81)
4	**2**	(0.000, -142.40)	(0.000, 62.74)	(-0.000, -14.65)
4	**3**	(0.000, -158.71)	(0.000, 1.57)	(-0.000, 18.89)
4	**4**	(0.000, 62.72)	(0.000, 93.37)	(-0.000, 3.69)

Table S7. Calculated spin-orbit coupling matrix elements between triplets (T) and singlets (S) using ωB97x-D4 functional. for the complex **Ir-bb**.

Root		$\langle \mathrm{T} \vert \mathrm{H_{SO}} \vert \mathrm{S} \rangle$ **(Re, Im) / cm^{-1}**		
T	**S**	**Z**	**X**	**Y**
1	**0**	(0.000, -148.63)	(0.000, 79.42)	(-0.000, 7.82)
1	**1**	(0.000, -103.64)	(0.000, 80.91)	(-0.000, -105.70)
1	**2**	(0.000, 318.76)	(0.000, -774.17)	(-0.000, 227.13)
1	**3**	(0.000, -533.21)	(0.000, -573.95)	(-0.000, -663.25)
1	**4**	(0.000, -17.07)	(0.000, 58.68)	(-0.000, 0.65)
2	**0**	(0.000, -62.80)	(0.000, 95.77)	(-0.000, -56.32)
2	**1**	(0.000, -496.40)	(0.000, 534.88)	(-0.000, -447.33)
2	**2**	(0.000, -289.16)	(0.000, 172.50)	(-0.000, 140.06)
2	**3**	(0.000, -193.28)	(0.000, -184.97)	(-0.000, 932.40)
2	**4**	(0.000, 37.47)	(0.000, -45.18)	(-0.000, 25.16)
3	**0**	(0.000, 63.92)	(0.000, -239.19)	(-0.000, 190.56)
3	**1**	(0.000, 8.94)	(0.000, 72.71)	(-0.000, 59.35)
3	**2**	(0.000, 197.64)	(0.000, -442.15)	(-0.000, 74.95)
3	**3**	(0.000, -352.19)	(0.000, -389.23)	(-0.000, -494.21)
3	**4**	(0.000, -6.59)	(0.000, 11.35)	(-0.000, -21.18)
4	**0**	(0.000, -85.36)	(0.000, 78.75)	(-0.000, -579.70)
4	**1**	(0.000, 265.50)	(0.000, 845.25)	(-0.000, 638.87)
4	**2**	(0.000, 353.34)	(0.000, 421.58)	(-0.000, -556.46)
4	**3**	(0.000, -167.28)	(0.000, -182.13)	(-0.000, 375.48)
4	**4**	(0.000, -71.13)	(0.000, -137.69)	(-0.000, 28.60)

Supplementary Notes S8: Lifetime of the emitter state

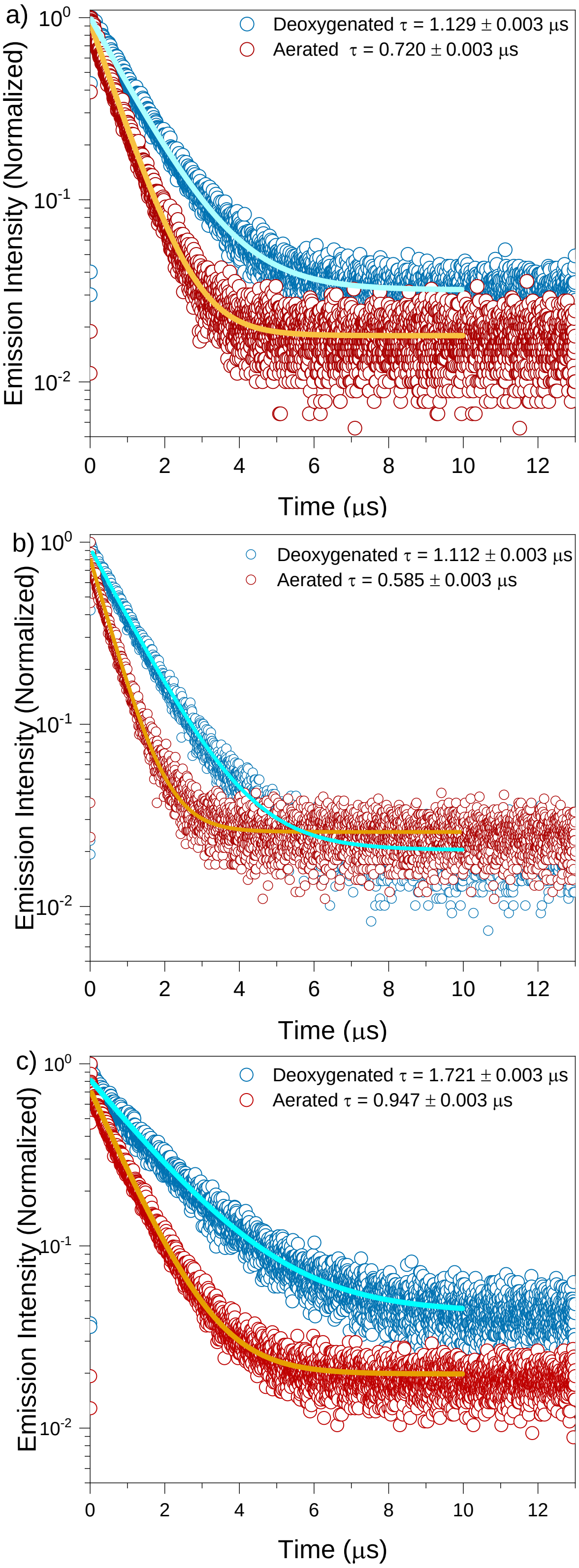

Fig. S12. Decay curves of the ^{3}LC-^{1,3}MLCT hybrid emitter state for the three Ir^{III} complexes in aerated and deoxygenated DMSO solution 1.0×10^{-5} mol L^{-1} at 298 K under pulsed NanoLED at 376 nm. **Ir-pb** (a), **Ir-qb** (b), and **Ir-bb** (c).

Supplementary Notes S9: Excited State Dynamics

In this section, some important theoretical aspects to the determination and comprehension of the photophysical properties of the three reported complexes are highlighted. Theoretical studies on transition metal complexes are quite common in the literature; however, for elements with higher atomic number, such as third-row transition metals, the corresponding properties are quite difficult to elucidate from routine calculations, due to the high atomic number[4]. At this point, the state-of-the-art single-reference approach to these compounds encompasses a full-relativistic treatment,[5] which was used in all the theoretical investigation available in this study.

Radiative Decay Rates

In Ir^{III} complexes, the excited-state (ES) radiative decay rate is often associated to the phosphorescence rate, accounting for transitions of the triplet ES to the singlet ground-state (GS).[6] In fundamental spectroscopy, a triplet-to-singlet transition is formally forbidden by the spin selection rule; however, the high spin-orbit coupling (SOC) in the Ir^{III} centre relaxes this rule by mixing states with distinct multiplicity.[6] In this context, the triplet level is split into three sublevels related to the spin projection, Fig. S13(a) for singlet pair and S13(b) for triplet pairs.

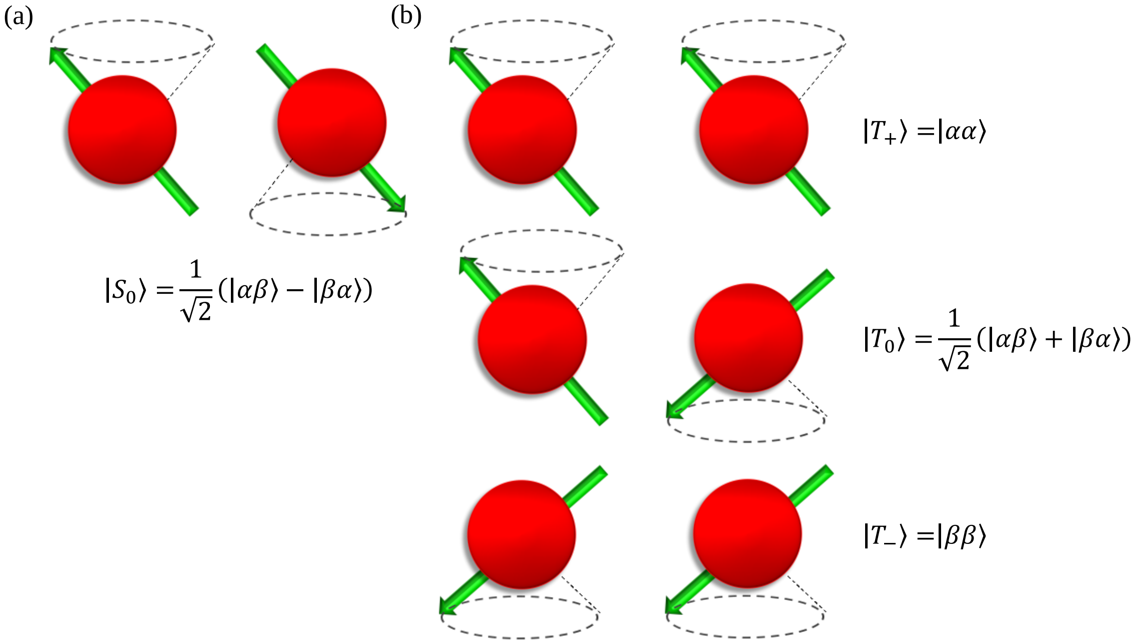

Fig. S13. Spin projection for (a) singlet state and (b) the three sublevels of triplet state.

In our calculations, this splitting was considered from the first-order full-SOC perturbation approach, whereas the singlet character was incorporated into the substates by second-order perturbation, leading to a non-null transition dipole moment.[6] Therefore, the expressions analysed by Yersin, *et al* in ref.[7] were adapted to include the density functional theory calculated properties, Eq. (S1), with the triplet state energy (*E(T*$_m$*)*), the singlet-triplet energy gap *(*$\Delta E(S_n - T_m)$), refractive index of the media (η), spin-orbit coupling matrix elements ($\langle T_1^\alpha | \hat{H}_{SOC} | S_n \rangle$), and transition dipole moment (M_{S_n}). The last is detailed in Eq. (S2), which was combined with Eq. (S1), resulting in the final expression, Eq. (S3), where the first term is reduced to $2\eta^3 E(T_m)^3/3$. Thus, the values of the SOC matrix elements are summarized in Table S3-S5, which were used to derive the numerical radiative decay rate.

$$k_r^\alpha(T_m \rightarrow S_n) = \frac{8\pi^2 \times 10^6 E(T_1)^3 \eta^3}{3\hbar\varepsilon_0} \left\{ \sum_n \frac{\langle S_n | \hat{H}_{SOC} | T_m^\alpha \rangle}{E(S_n) - E(T_m)} M_{S_0} \right\}^2 \quad \text{Eq. (S1)}$$

$$M_{S_n} = \frac{e}{2} \sqrt{\frac{3\hbar}{\pi m_e c} \times \frac{f_n}{E(S_n)}} \quad \text{Eq. (S2)}$$

$$k_r^\alpha(T_m \rightarrow S_n) = \frac{2\pi \times 10^6 E(T_1)^3 \eta^3 e^2}{m_e \varepsilon_0 c} \left\{ \sum_n \frac{\langle S_n | \hat{H}_{SOC} | T_m^\alpha \rangle}{E(S_n) - E(T_m)} \right\}^2 \times \frac{f_n}{E(S_n)} \quad \text{Eq. (S3)}$$

These matrix elements were determined from applying the spin-orbit mean field (SOMF) approximation, which expresses the Breit-Pauli (BP) operator approximately as an effective one-electron operator, where the used matrix elements are obtained from the reduced ones, representing each substate in Eqs. (S4).[8] The Eq. (S4a) denotes the $M_S = -1$ (x), Eq. (S4b) the $M_S = 0$ (y), and Eq. (S4c) the $M_S = +1$ (z), in which M_S accounts for the spin projection quantum number.

$$Y_{IJ}^{SS-1}(m) = \left\langle \Psi_I^{SS} \middle| \textstyle\sum_i \hat{z}_m(i)\, \hat{s}_{+1}(i) \middle| \Psi_J^{S-1S-1} \right\rangle \quad \text{Eq. (S4a)}$$

$$Y_{IJ}^{SS}(m) = \frac{\sqrt{S(S+1)}}{S} \left\langle \Psi_I^{SS} \middle| \textstyle\sum_i \hat{z}_m(i)\, \hat{s}_0(i) \middle| \Psi_J^{SS} \right\rangle \quad \text{Eq. (S4b)}$$

$$Y_{IJ}^{SS+1}(m) = \sqrt{\frac{2S+3}{2S+1}} \left\langle \Psi_I^{SS} \middle| \textstyle\sum_i \hat{z}_m(i)\, \hat{s}_{-1}(i) \middle| \Psi_J^{S+1S+1} \right\rangle \quad \text{Eq. (S4c)}$$

Non-Radiative Decay Rates

The energy gap law states that by decreasing the energy difference between the ground and the emitting excited state the non-radiative decay rate (k_{nr}) increases, also enhancing the probability of vibrational quenching.[4] For an electronic transition, the emission spectrum can be described as an envelope of vertical transitions linking the electronically excited and ground states, while its intensity is calculated using the Franck-Condon (FC) principle, whose factors measure the overlap magnitude.[9]

In this scenario, the FC factors are influenced by the vibrational modes, which displace the atomic coordinates from the equilibrium position (Q) to Q+dQ.[9] Consequently, the non-radiative decay rates can be calculated by adapting the Fermi's golden rule, shown in Eq. (S5), where *F* is associated with the spectral overlap between the functions,[10] leading to Eq. (S6a), which is decomposed into a convenient numerical expression, Eq. (S6b).[11] In such cases, ΔE_{00} is the zero-point energy difference between the T_1 and S_0 states, n_M is the number of quanta of the effective high frequency mode $\hbar\omega$, S_j is the Huang-Rhys factor corresponding to the equilibrium displacement of the *j*-th normal mode ω_j, and S_M is defined in Eq. (S6c), as the sum of the Huang-Rhys factors in high frequency modes.[11]

To obtain the k_{nr} the following assumptions were made: (*i*) the MLCT transition changes the electron density upon the metal ion and ligand, under the same pattern, $\omega_j^S \neq \omega_j^{S(T)}$; (*ii*) the low frequency modes ($\omega_{lf} \leq 1000$ cm^{-1}) are treated in the strong coupling limit when the Huang-Rhys factor exceeds the unit value ($S_{lf} \gg 1$). In contrast, the high frequency skeletal modes ($1700 \leq \omega_{hf} \leq 1000$ cm^{-1}) are treated under the weak coupling limit, requiring $S < 1$ or $\hbar\omega_M \gg k_B T$. Therefore, the parameters that describe the thermally-average FC factors in Eq. (S6b) are presented in Eq. (S6c – h).

$$k_{nr} = \frac{2\pi}{\hbar} \left|\left\langle T_1 \middle| \widehat{H}_{SOC} \middle| S_0 \right\rangle\right|^2 F \quad \text{Eq. (S5)}$$

$$k_{nr}(T_1 \longrightarrow S_0) = \left(\frac{\left\langle T_1 \middle| \widehat{H}_{SOC} \middle| S_0 \right\rangle}{\hbar}\right)^2 \int f(t) exp\left(-\frac{i\left|E_{V_T}(T_1) - E_{V_S}(S_0)\right|}{\hbar}\right) dt \quad \text{Eq. (S6a)}$$

$$k_{nr}(T_1 \longrightarrow S_0) = 2\pi \frac{\left\langle T_1 \middle| \widehat{H}_{SOC} \middle| S_0 \right\rangle^2}{\hbar^2} \left[2\pi\hbar^2(D_1^2 + P^2)\right]^{-\frac{1}{2}} exp\left[\left(\frac{(\Delta E_{00} - n_M\hbar\omega_M - \lambda_1 - \mu)}{2\pi\hbar^2(D_1^2 + P^2)}\right) - \left(\frac{(\Delta E_{00} - n_M\hbar\omega_M - \lambda_1 - \mu)}{2\pi\hbar^2(D_1^2 + P^2)}\right)\right] \quad \text{Eq. (S6b)}$$

$$S_j = \frac{1}{2}\omega_j(\Delta Q_e)^2;\ S_M = \sum_{j\epsilon lf} S_j \quad \text{Eq. (S6c)}$$

$$b_j = \frac{\omega_j^T}{\omega_j^S} \quad \text{Eq. (S6d)}$$

$$\hbar^2 D_1^2 = \sum_{j\in lf} S_j \left(\frac{\hbar\omega_j^S}{b_j}\right)^2 coth\frac{\hbar\omega_j^T}{2K_BT};\ \hbar^2P^2 = \frac{1}{2}\sum_{j\in lf}\left[\hbar\omega_j^S\frac{1-b_j^2}{b_j}coth\frac{\hbar\omega_j^T}{2K_BT}\right]^2 \quad \text{Eq. (S6e)}$$

$$\lambda_M = \sum_{j\in lf} S_j\hbar\omega_j\ ;\ \hbar\omega_j = \frac{\lambda_M}{S_M};S_M = \sum_{j\in lf} S_j\ ;\ \lambda_1 = \sum_{j\in lf}\frac{S_j\hbar\omega_j^S}{b_j} \quad \text{Eq. (S6f)}$$

$$\mu = \frac{1}{2}\sum_{j\in lf}\hbar\omega_j^S\frac{1-b_j^2}{b_j}coth\frac{\hbar\omega_j^T}{2K_BT} \quad \text{Eq. (S6g)}$$

$$n_M = \frac{\Delta E_{00} - \lambda_1 - \mu}{\hbar\omega_M} \quad \text{Eq. (S6h)}$$

From these equations, three major factors that coordinate the non-radiative decay rates are highlighted. First, the SOC matrix elements, second, the effective energy gap ($\Delta E' = \Delta E_{00} - \lambda_1 - \mu$), and third, the Huang-Rhys parameter (S). By increasing the SOC matrix elements one strengthens the k_{nr} due to a direct proportionality, while an inverse proportionality is noted between the effective gap and the k_{nr}. Lastly, it is known that S is proportional to the reorganization energy, **λ,** associated with structural distortions (Fig S14). Thus, increasing the equilibrium displacement augments the k_{nr} values.

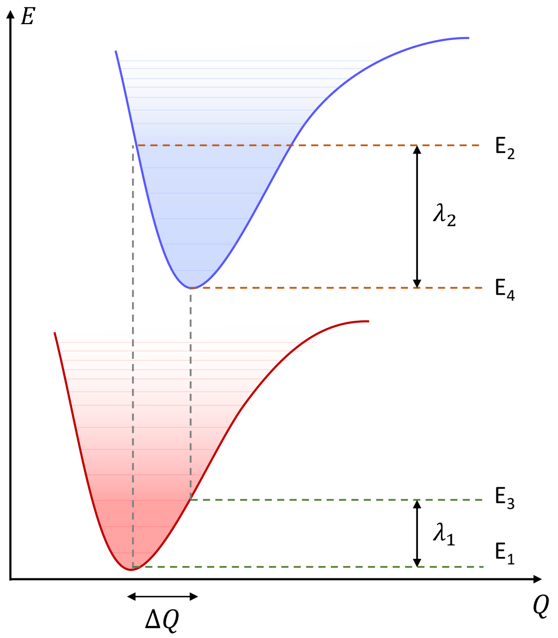

Fig. S14. Atomic displacement and reorganization energy for the excited and the ground-states.

In this context, the optimized ground and excited state geometries of each complex were superimposed in Fig. 5, where the deviation of both structures (ΔQ) is related to the reorganization energy. The augment of the deviation leads to higher non-radiative deactivation according to Eq. S6b due to the inverse exponential dependence of k_{nr} with the difference between the energy of the 0-0 phonon line (ΔE_{00}) and the reorganization energy. Within this approach, as the values of λ_{RE} approach ΔE_{00}, the exponent tends to unity, and k_{nr} will only depend on the SOCMEs, the energy of vibrational modes and its corresponding Huang-Rhys factor. Therefore, the trend in the λ_{RE} agrees with both theoretical and experimental values of k_{nr}, as shown in the main text. Additionally, we highlight the vibrational modes used in these calculations for each complex (Fig S15). The absence of imaginary frequencies in all three compounds for both S_0 and T_1 structures implies that we used all compounds at their local minima, i.e, the optimized geometries.

For red-emitting Ir^{III} compounds, by increasing the geometric distortion of the emissive state related to the ground state the quenching by vibrational coupling increases.[7] Thus, further strategies to inhibit the distortions are being developed, such as enhancing the molecular rigidity to reduce the Huang-Rhys parameter.

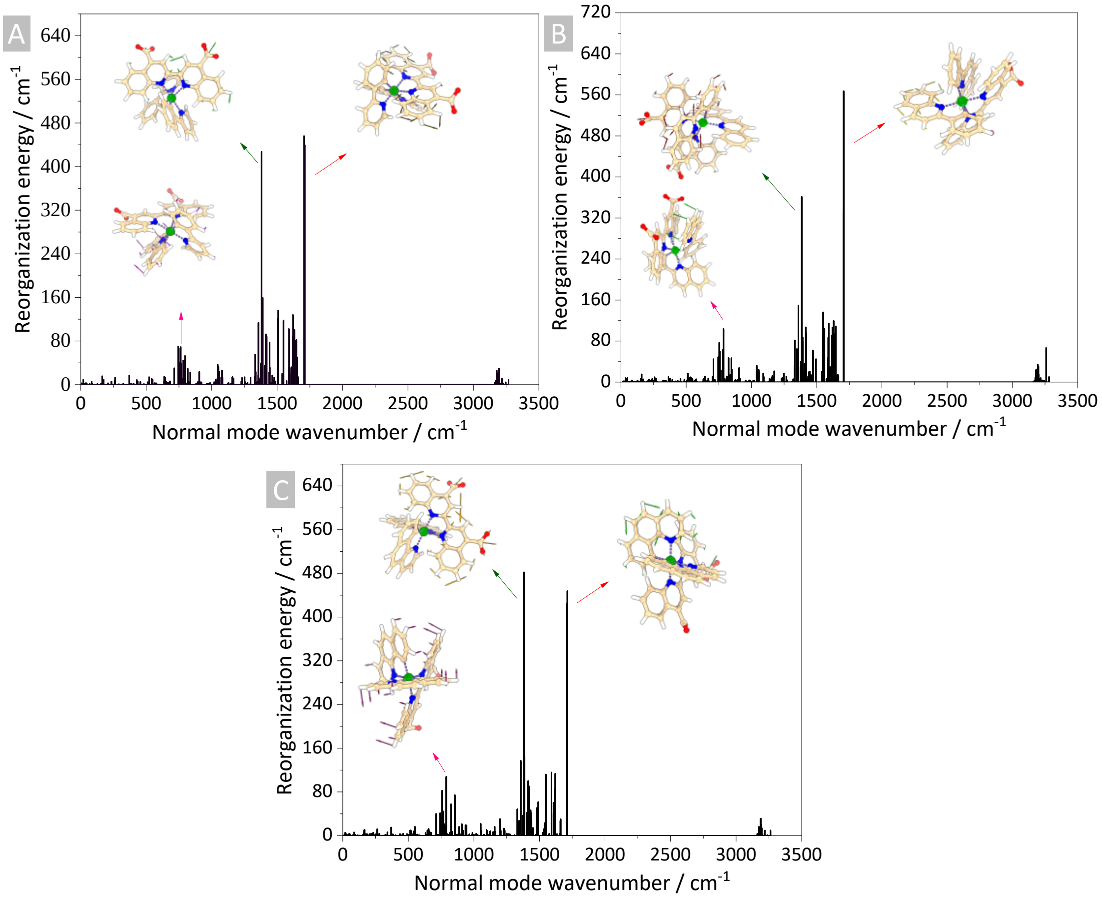

Fig. S15. Reorganization energy in terms of the normal mode wavenumber, calculated from the normal mode force constant using the harmonic oscillator model for **Ir-pb** (a), **Ir-qb** (b), and **Ir-bb** (c).

Supplementary Note S10: Script to Radiative Decay

```
# Script to calculate the radiative decay rates
# Laboratory of Luminescence in Materials and Sensors (LLuMeS) / Leonardo
F Saraiva

import os
import numpy as np
from numpy import sqrt

# Defining the functions to compute the radiative decay

# Function to input the refractive index due to its cube dependence

def reffractive_index():

    while True:
        print("**********************************************************
**********************")
        print("**********************************************************
**********************")
        print("**
                   **")
        print("**
                   **")
        print("**        Laboratory of Luminescence in Materials and
Sensors - LLuMeS        **")
        print("**                           Leonardo F
Saraiva                               **")
        print("**
                   **")
        print("**
                   **")
        print("**********************************************************
**********************")
        print("**********************************************************
**********************")
        media = input("Enter the used media (chloroform \ dichloromethane
\ acetonitrile \ DMSO \ ethanol \ other): ")
        valid_responses = ["chloroform", "dichloromethane",
"acetonitrile", "DMSO", "ethanol", "other"]
        if media == "other":
            print("The media you are using is not predefined")
        else:
            print("The media you are using is: " + media)
        if media not in valid_responses:
            print("chloroform, dichloromethane, acetonitrile, DMSO and
ethanol only")
        else:
```

```
            if media == "chloroform":
                print("You are using the refractive index of 1.4459")
                return 1.4459
            elif media == "dichloromethane":
                print("You are using the refractive index of 1.4241")
                return 1.4241
            elif media == "acetonitrile":
                print("You are using the refractive index of 1.3441")
                return 1.3441
            elif media == "DMSO":
                print("You are using the refractive index of 1.4793")
                return 1.4793
            elif media == "ethanol":
                print("You are using the refractive index of 1.3610")
                return 1.3610
            else:
                media_1 = float(input("Input here the refractive index: "))
                return media_1


# Defining function to input the energy of T1

def triplet_energy():
    while True:
        energy_T = float(input("Enter here the triplet state energy in (1/cm): "))
        try:
            if energy_T > 0:
                break
            else:
                print("Enter a positive energy value!")
        except ValueError:
            print("Amount must be a number!")
    return energy_T

# Defining function to input the energy of S0
# Note that S0 -> 0 in all cases, but S0 != 0 due to the denominator

def singlet_energy():
    while True:
        energy_S = float(input("Enter here the singlet state energy in (1/cm): "))
        try:
            if energy_S > 0:
                break
            else:
                print("Enter a positive energy value!")
        except ValueError:
            print("Amount must be a number!")
```

```
    return energy_S

# Defining function to input the oscillator strength
# If T1 is not well-defined, the mean oscillator strength needs to be used

def oscillator_strength():
    while True:
        oscillator = float(input("Enter here the oscillator strength: "))
        try:
            if oscillator > 0:
                break
            else:
                print("Enter a positive energy value!")
        except ValueError:
            print("Amount must be a number!")
    return oscillator

# Input the SOCMEs.
# SOCMEs for Ir3+ should be in the 1E2 order.

def matrix_elements():
    soc_component = None
    matrix = input("Do you want to include the SOC effect? (Y/N): ")
    if matrix.lower() == "y":
        element_x = float(input("Input the elements on the x axis: "))
        element_y = float(input("Input the elements on the y axis: "))
        element_z = float(input("Input the elements on the z axis: "))
        print(f"The elements are:\nx = {element_x}\ny = {element_y}\nz = {element_z} ")
        soc_component = (element_x, element_y, element_z)
    elif matrix.lower() == "n":
        print("SOC is not considered")
        element_x = 0.0
        element_y = 0.0
        element_z = 0.0
        soc_component = (element_x, element_y, element_z)
    else:
        print("Invalid input. Please enter Y or N")
    return soc_component

# In case the calculation was performed in a software that does not accomplish\n
# the SOCMEs, it can be approximated by the SOC constant\n
# and the coefficients. See: https://doi.org/10.1039/C8RA02858C
# To use this section remove the "#" from def matrix_Ir()\n
# insert "#" in front of def matrix_elements():

# def matrix_Ir():
    while True:
```

```
        matrix = input("Do you want to include SOC effects? (Y/N)")
        if matrix == "y":
            coefficient_1 = float(input("Enter the singlet mixing coefficient "))
            coefficient_2 = float(input("Enter the triplet mixing coefficient "))
            SOC_constant = float(input("Enter the SOC constant in (1/cm) "))
            matrix_elements_real = coefficient_1 * coefficient_2 * (0.5 * SOC_constant)
            arr = sqrt(-1)
            matrix_elements_imaginary = coefficient_1 * coefficient_2 * (0.5 * arr * SOC_constant)
        if matrix == "n":
            break
    return matrix_elements_real, matrix_elements_imaginary

# Main function to calculate the radiative rates

def main():
    ref = reffractive_index()  # remove float() conversion
    triplet = float(triplet_energy())
    singlet = float(singlet_energy())
    oscillator = float(oscillator_strength())
    matrix_x, matrix_y, matrix_z = matrix_elements()  # fix variable name and unpack return values
    calc_1 = (((ref**3) * (triplet**3) / 1.5) * ((matrix_x) / (singlet - triplet))**2 * (oscillator / singlet))
    calc_2 = (((ref**3) * (triplet**3) / 1.5) * ((matrix_y) / (singlet - triplet))**2 * (oscillator / singlet))
    calc_3 = (((ref**3) * (triplet**3) / 1.5) * ((matrix_z) / (singlet - triplet))**2 * (oscillator / singlet))
    calc = ((calc_1 + calc_2 + calc_3) / 3)
    print(f"The theoretical average radiative decay rate for your complex is: {calc}")

main()
```

References

1 I. S. Kritchenkov, V. G. Mikhnevich, V. S. Stashchak, A. I. Solomatina, D. O. Kozina, V. V. Sokolov and S. P. Tunik, *Molecules*, 2022, **27**, 3153–3153.

2 T. Yoshihara, S. Murayama, T. Masuda, T. Kikuchi, K. Yoshida, M. Hosaka and S. Tobita, *J Photochem Photobiol A Chem*, 2015, **299**, 172–182.

3 T. M. Stonelake, K. A. Phillips, H. Y. Otaif, Z. C. Edwardson, P. N. Horton, S. J. Coles, J. M. Beames and S. J. A. Pope, *Inorg Chem*, 2020, **59**, 2266–2277.

4 X. Zhou and B. J. Powell, *Physical Chemistry Chemical Physics*, 2020, **22**, 27348–27356.

5 F. Neese, *Journal of Chemical Physics*, 2005, **122**, 034107.

6 K. Mori, T. P. M. Goumans, E. Van Lenthe and F. Wang, in *Physical Chemistry Chemical Physics*, Royal Society of Chemistry, 2014, vol. 16, pp. 14523–14530.

7 H. Yersin, A. F. Rausch, R. Czerwieniec, T. Hofbeck and T. Fischer, *Coord Chem Rev*, 2011, **255**, 2622–2652.

8 F. Neese, T. Petrenko, D. Ganyushin and G. Olbrich, *Coord Chem Rev*, 2007, **251**, 288–327.

9 P. Herr and O. S. Wenger, *Inorganics (Basel)*, 2020, **8**, 1–11.

10 A. N. Carneiro Neto, E. E. S. Teotonio, G. F. de Sá, H. F. Brito, J. Legendziewicz, L. D. Carlos, M. C. F. C. Felinto, P. Gawryszewska, R. T. Moura, R. L. Longo, W. M. Faustino and O. L. Malta, *Handbook on the Physics and Chemistry of Rare Earths*, 2019, **56**, 55–162.

11 Y. Chen, A. Ren, Z. Yang, T. He, X. Ding, H. Zhang and L. Zou, *Physical Chemistry Chemical Physics*, 2018, **20**, 9419–9428.